Metallophysics and Advanced Technologies
Металофіз. новітні технол.
Metallofiz. Noveishie Tekhnol.
2025, vol. 47, No. 3, pp. 287–301
https://doi.org/10.15407/mfint.47.03.0287
Reprints available directly from the publisher

PACS numbers: 62.20.Qp, 62.25.Mn, 75.50.Kj, 81.20.Ev, 81.40.Ef, 81.40.Lm, 81.40.Rs

The Effect of Heat Treatment on the Physical and Mechanical Properties, and Grindability of the Amorphous $Fe_{73}Si_{16}B_7Cu_1Nb_3$ Alloy Ribbon

B. S. Baitaliuk, V. K. Nosenko, and I. K. Yevlash

G. V. Kurdyumov Institute for Metal Physics, NAS of Ukraine,
36 Academician Vernadsky Blvd.,
UA-03142 Kyiv, Ukraine

The effect of heat treatment on the physical and mechanical properties and grindability of amorphous $Fe_{73}Si_{16}B_7Cu_1Nb_3$ (of FINEMET-type) alloy ribbon is investigated. A non-monotonic dependence of microhardness, brittleness, and electrical resistivity on the annealing temperature is established. As shown, the optimum temperature, which provides the best grindability of the ribbon, is of 450°C, which is lower than the nanocrystallization temperature of this amorphous alloy. The morphology, size, and fractional composition of the grinded powder are studied using scanning electron microscopy.

Key words: FINEMET, amorphous ribbon, nanocrystalline structure, heat treatment, powder.

Досліджено вплив термічного оброблення аморфної стрічки стопу $Fe_{73}Si_{16}B_7Cu_1Nb_3$ (типу FINEMET) на фізико-механічні властивості та здатність до подрібнення. Встановлено немонотонну залежність мікротвердости, крихкости, електроопору від температури відпалу. Показано, що оптимальною температурою, яка забезпечує найліпше подрібнення стрічки є температура у 450°C, що є нижчою за температуру нанокристалізації цього аморфного стопу. З використанням електронної сканувальної мікроскопії досліджено морфологію, розміри та фракційний склад подрібненого порошку.

Ключові слова: FINEMET, аморфна стрічка, нанокристалічна структура, термооброблення, порошок.

Corresponding author: Bohdan Serhiyovych Baitaliuk
E-mail: baytalyuk@ukr.net

Citation: B. S. Baitaliuk, V. K. Nosenko, and I. K. Yevlash, The Effect of Heat Treatment on the Physical and Mechanical Properties, and Grindability of the Amorphous $Fe_{73}Si_{16}B_7Cu_1Nb_3$ Alloy Ribbon, *Metallofiz. Noveishie Tekhnol.*, **46**, No. 3: 287–301 (2024). DOI: 10.15407/mfint.47.03.0287

(Received 30 July, 2024; in final version, 1 August, 2024)

1. INTRODUCTION

Modern electronic and electrotechnical devices cannot do without inductive components such as inductors, filters, transformers, and sensors. These components often include magnetodielectrics as the basis for magnetic cores, especially considering modern trends towards miniaturization and high efficiency in electronics and microelectronics [1–8].

Along with traditional materials for the production of magnetodielectrics, which have been actively used for a long time (these are composites mainly based on iron, Sendust, Permalloy, Fe–Si system alloys and their mixtures [9–17]), composites based on powders of amorphous and nanocrystalline alloys are becoming increasingly widespread [18–23]. Alloys based on iron, cobalt, and nickel have become widely used, primarily due to their high saturation induction and low hysteresis and eddy current losses [24–27].

Among the new materials used in the production of magnetodielectrics is the FINEMET alloy, which is essentially an amorphous Fe–Si–B alloy with small admixtures of Cu and Nb [28]. The optimal composition of the alloy has hardly changed since its invention—it is $Fe_{73.5}Si_{13.5}B_9Cu_1Nb_3$ [29]. This unusual combination of elements has become the key to obtaining a nanocrystalline structure with high soft magnetic properties [30, 31].

The results of numerous studies [32–39] have shown that magnetodielectrics based on this type of alloy are today increasingly being offered with a wide range of properties according to the field of application to replace expensive Permalloy cores. The combination of high saturation induction, high permeability, good frequency dependence, low hysteresis losses and temperature stability allows reducing the weight and dimensions of the magnetic components used, for example, in pulse power supplies or telecommunications equipment. In addition to these attractive characteristics, the nanocrystalline alloy is made from inexpensive iron and silicon. All this together has led to a constantly growing application of the new alloy in magnetic choke cores, high-frequency transformers, inductors and converters for various fields of electronics and electrical engineering.

For the production of massive magnetodielectrics of various shapes and sizes, powder metallurgy methods [40–43] are mainly used, which include the following basic operations: production of powders, mixing with a binder, pressing, sintering, finishing operations. An important stage in the production of magnetodielectrics, based on nanocrystalline alloys, is the process of powders production. Physical, physical-mechanical, and magnetic properties of obtained products great extent

depend on powder performances [44].

Attempts to obtain powders from amorphous and nanocrystalline alloys have been made repeatedly [45–47]. Among the known works, those [48–53] deserve attention, in which the authors achieved the goal by mechanically grinding an amorphous or nanocrystalline ribbon. Thus, the authors of [32] obtained composites based on powders of the nanocrystalline alloy FINEMET. The powder was obtained by grinding a pre-annealed amorphous ribbon at a temperature of 573 K to make it brittle. However, along with describing all the advantages of this method, the authors limited themselves to a separate study of technological properties and practically did not consider the influence of the annealing temperature on the grindability of the ribbon, as well as such characteristics of the powder as particle size, shape, electrical resistivity, and hardness, which is important for further study of the process of forming magnetic cores from nanocrystalline powders.

In this work, the results of studying the effect of the annealing temperature of the amorphous ribbon of the $Fe_{73}Si_{16}B_7Cu_1Nb_3$ alloy (MM-11H [54]) on its plasticity, microhardness, electrical resistivity, and grindability are presented. Obtaining an amorphous powder by grinding waste from the production of an amorphous ribbon has obvious advantages and does not require complex technological equipment for its production. The powder obtained by this method has a homogeneous structure and composition, as well as minimum impurity content, which is difficult to achieve when manufacturing amorphous powder by other methods (for example, spraying or mechanical synthesis).

2. OBJECTS AND RESEARCH METHODS

Non-conforming remnants of the amorphous ribbon of the MM-11H alloy (manufactured by LLC 'MELTA') with the composition $Fe_{73}Si_{16}B_7Cu_1Nb_3$, 20 μm thick and 10 mm wide (Fig. 1), were used as the starting material for the research.

To obtain the powder and study the grindability of the ribbon, a ball mill was used, and the grinding parameters are given in Table 1.

The shape and morphology of the surface of individual powder particles were determined using a РЕМ-106*И* scanning electron microscope.

The microhardness of the ribbon was measured on ПМТ-3 microhardness meter using the Vickers method (ГОСТ ISO 6507-1:2007). The hardness value was calculated by the formula:

$$H = 1854P/d^2, \quad (1)$$

where P is the load (g), d is the diagonal of the imprint (μm).

The electrical resistance of the samples was measured using a CS4105 microohmmeter, designed to measure electrical resistance in

Fig. 1. Non-conforming remnants of the studied amorphous alloy MM-11H ribbon.

the range from 10^{-5} to 50 Ω.

To determine the brittleness of the nanocrystalline ribbon, was used a method that was described in [56]. The essence of the method is that the ribbon is clamped between two micrometer jaws, as shown in Fig. 2, which is compressed until destruction.

Relative deformation before destruction in the surface zone of the ribbon is taken as the criterion of brittleness. The parameter of brittleness is the value ε_f:

TABLE 1. Technological parameters of obtaining powder of nanocrystalline alloy MM-11H by grinding in a ball mill. n_{cr} is the critical rotational speed of the mill, at which balls 'stick' to the drum walls [55].

Technological parameter	Optimal values	Used values	Notes
Drum diameter D, cm	–	20	Drum volume: 7.22 l
Drum rotation speed, rpm	$(0.75–0.8)n_{cr}$	95	$n_{cr} = 42.4D^{-1/2}$
Ball-to-material mass ratio	2.5–6	5.5	Ball mass: 12.2–13.7 kg
Mill filling coefficient	0.4–0.5	0.5	$V_{material}/V_{drum}$
Grinding environment	Alcohol	Alcohol	Contributes to the intensification of grinding
Grinding time, min	30–60	60	To obtain the desired fraction

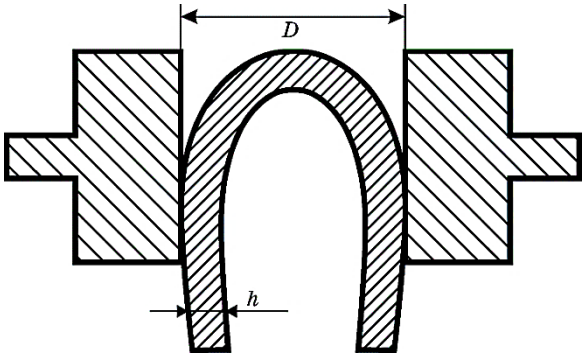

Fig. 2. Scheme of the installation for determining the brittleness of the nanocrystalline ribbon.

$$\varepsilon_f = h/(D - h), \tag{2}$$

where h is the thickness of the ribbon, D is the distance between the micrometer jaws between which the bending is carried out at the moment of the ribbon destruction.

The obtained values of ε_f were averaged over the data of 5 measurements, excluding the results in which the brittleness was several times higher than in most measurements.

The heat treatment of the amorphous ribbon was carried out at temperatures of 200–600°C in air, with a holding time of 30, 60, and 90 minutes for each individual experiment.

3. RESULTS AND DISCUSSION

3.1. Brittleness of the Ribbon

As known, pressing is an important stage in the manufacture of powder parts, including cores. The ability to compact powder samples is strongly influenced by the shape and plasticity of the powder particles, and to a lesser extent by the surface condition and the coefficient of friction between the particles and the walls of the mould. Since the shape of the powder particles produced by the mechanical grinding of the ribbon is always the same (plate-like, flaky), the main indicator of the ability of amorphous and nanocrystalline powders to deform can be the level of their plasticity (which can be indirectly judged by the level of their hardness). For powder soft magnetic composites, lower microhardness usually contributes to better compaction, higher strength, better magnetic properties of finished products, and less wear of mould parts during the forming process.

Additionally, it is worth noting that the choice of annealing temper-

ature and duration is of strategic importance. Annealing at low temperatures may not provide sufficient brittleness for effective grinding, while high temperatures can lead to unwanted boride crystallization and loss of magnetic properties. Thus, the ideal annealing temperature for the MM-11H alloy is in the range that provides optimal brittleness without the risk of crystallization.

At the first stage, the amorphous ribbon was subjected to heat treatment to increase its brittleness. For this purpose, it was annealed at temperatures of 200, 300, 450, 530 and 600°C for 30, 60 and 90 minutes (in air). It is not advisable to use high temperatures, since above 600°C for the studied alloy, rapid crystallization processes begin and it loses its magnetic properties [28, 57, 58].

To determine the grindability of the ribbon, the loss of its plasticity (embrittlement) as a function of the annealing temperature was investigated. A typical curve of the dependence of the brittleness of amorphous alloys on the annealing temperature is shown in Fig. 3.

It is easy to see in Fig. 3 and expression (2) that in a completely plastic state (when the ribbon bends without destruction) $D = 2h$ and $\varepsilon_f = 1$. The higher the value of D, the higher the degree of brittleness. In absolute brittleness, $D \to \infty$ and $\varepsilon_f \to 0$.

The dependence of the relative deformation to fracture of the MM-11H alloy ribbon on the annealing temperature and time is shown in Fig. 4.

The nature of the curve's behaviour shows that in the initial state, the amorphous ribbon has high plasticity, strength, and hardness, the absence of deformation hardening, and very small values of macroscopic deformation before destruction. However, after annealing at a temperature above a certain critical temperature, it transitions into a brittle state. This phenomenon of loss of plasticity within the amor-

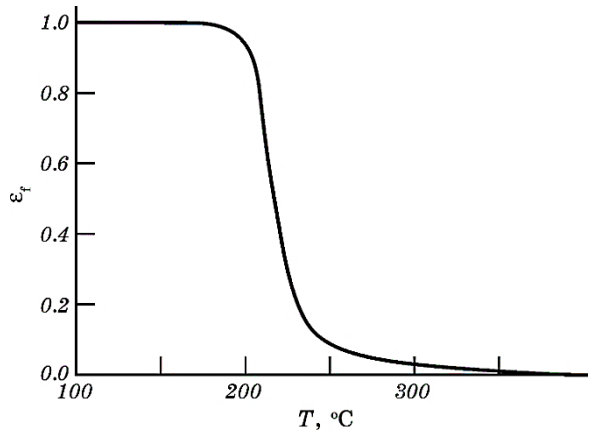

Fig. 3. Typical curve of the dependence of the brittleness of amorphous alloys on the annealing temperature [56].

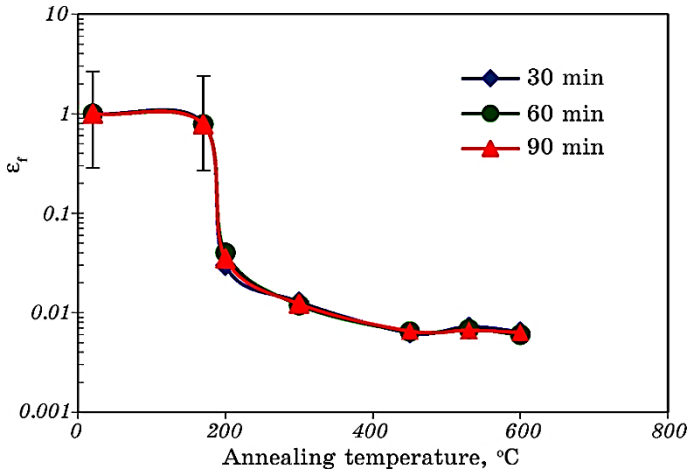

Fig. 4. Dependence of the relative deformation before destruction of the MM-11H alloy ribbon on the annealing temperature and time.

phous state is called annealing brittleness of amorphous alloys [59].

The transition temperature from the plastic state to the brittle state for the alloy under study is about 200°C, as can be seen from Fig. 4. It has been established that the annealing duration within 30–90 minutes does not affect the deformation value before destruction, since the alloy acquires these properties in the first minutes of annealing [56]. More accurate results of the acquisition of brittleness by the ribbon at the initial stages of crystallization do not seem possible due to the small thickness of the ribbon and the large error in measuring the fracture distance of less than 0.1 mm.

It is interesting that at a temperature of 530°C, a slight increase in plasticity is observed, and this change looks the same for each annealing time. This can be seen in detail from Fig. 5, where the distance (*D* in millimetres) at which the 20 μm thick ribbon breaks is plotted on the ordinate axis instead of the deformation value before destruction ε_f.

Such behaviour of the curves in amorphous-nanocrystalline Fe-based alloys can be caused by various factors such as crystallization, enrichment with soluble elements, phase separation, free volume annihilation, and residual stress. The exact cause of annealing brittleness remains is unknown [60].

The authors of [61] investigated the effect of annealing temperature on the mechanical and structural transitions of the nanocrystalline Fe–Si–B alloy ribbon. They concluded that the initial drop in plasticity could be explained by the release of free volume and an increase in the volume of the shear transformation zone volume. The release of free volume leads to structural relaxation of residual stresses. In addition, a slight dip in the brittleness curve in the crystallization temperature

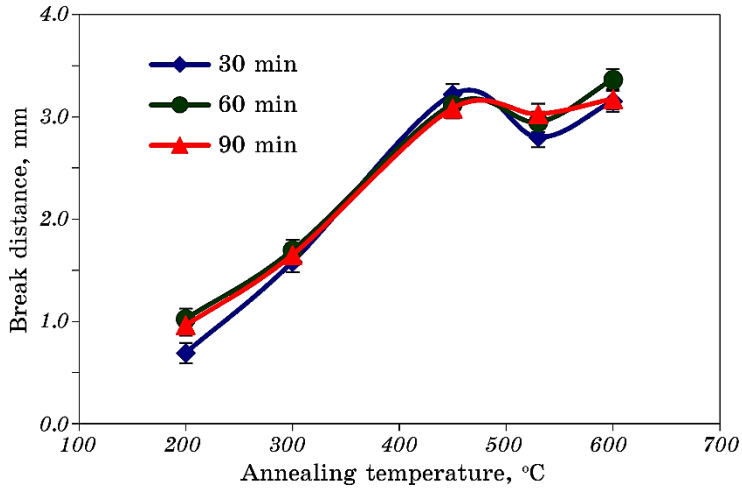

Fig. 5. Dependence of the fracture distance of the 20 μm thick MM-11H alloy ribbon on the annealing temperature and time.

range is due to the very beginning of nanocrystallization and a decrease in internal stresses.

In our case, at a temperature of 530–570°C, nanocrystallization of the alpha-solid solution of silicon in iron (with a b.c.c. lattice) occurs rapidly [28, 57]. The general microstructure is characterized by randomly oriented ultrathin grains of b.c.c. Fe(Si) (20 at.% Si) with an average grain size of 10–15 nm within the amorphous matrix, which occupies 20–25% of the total volume of the ribbon. This structure is the basis for unique soft magnetic properties.

It should be noted that the optimal volume ratio between iron nanocrystals and the amorphous matrix is not achieved immediately, nor is the optimal silicon content in nanocrystals. It is achieved after a certain period of time and at a certain optimal temperature, which, due to the intense mechanical effect on the initial structure of the ribbon, may change for the ground powder compared to the ribbon.

3.2. Microhardness of the Ribbon

Figure 6 shows the dependence of the microhardness of the MM-11H ribbon on the annealing temperature and time.

As can be seen in Fig. 6, at annealing temperatures up to 450°C, the microhardness of the ribbon almost does not change (in comparison with the initial state) and reaches ≅ 800 kg/mm^2. Starting from a temperature of 450°C, the microhardness of the alloy begins to grow rapidly and increases almost twice by the time it reaches 600°C. Moreover, the annealing time within 30–90 minutes does not affect the hardness

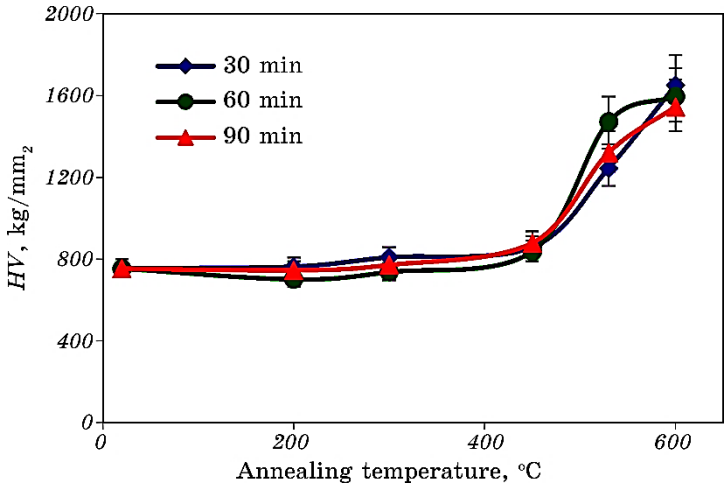

Fig. 6. Dependence of the microhardness of the MM-11H alloy ribbon on the annealing temperature and time.

in any way (the slight discrepancy in values can be explained by the measurement error).

A characteristic feature of the MM-11H alloy is also that the microstructure (as well as the soft magnetic properties) does not strongly depend on the annealing temperature (T_a) in the range $\Delta T_a = 50–100$°C. The main process takes place in the first 10–15 minutes and does not strongly depend on the subsequent nanocrystallization time. However, increasing the annealing temperature above approximately 600°C leads to both rapid growth of nanograins to micron sizes and crystallization of the residual amorphous phase with the formation of Fe_2B and Fe_3B borides [28, 57, 62].

3.3. Electrical Resistivity of the Ribbon

One of the important properties that magnetodielectrics must have is high specific electrical resistivity. The low eddy current losses of amorphous and nanocrystalline alloys are due to the fact that they have a relatively lower specific electrical conductivity, in particular, compared to pure iron, electrical steels or Permalloys.

As is known, losses in magnetic materials are divided into three categories:

$$P = P_h + P_e + P_{ex}, \tag{3}$$

where P_h is hysteresis loss, P_e is eddy current loss, P_{ex} is excess loss.

The nature of excess losses is not yet well understood. These losses

depend on the mechanical stresses arising in the material and resonant losses. They appear at very low induction values and very high frequencies, so these losses are usually ignored. Therefore, the main losses in the core are hysteresis losses and eddy current losses.

The dependence of the electrical resistivity of the MM-11H alloy ribbon on the annealing temperature is shown in Fig. 7.

Figure 7 shows that in the unannealed state, the ribbon has an electrical resistivity of $1.9 \cdot 10^{-6}$ μΩ·m, which is consistent with the literature data for amorphous ribbons: 100–300 μΩ·cm, including the review work by the authors [63]. This is an order of magnitude higher than that of pure iron ($0.1 \cdot 10^{-6}$ μΩ·m), and much higher than that of electrical steels (0.25–0.6 μΩ·m), Sendust (0.8 μΩ·m), molybdenum Permalloy (0.6 μΩ·m), and iron–nickel Permalloy (0.45 μΩ·m), which are often used as magnetic conductors. The electrical resistivity of the MM-11H amorphous ribbon even exceeds the values of nichrome (1.1 μΩ·m) or FeCrAl (1.2–1.4 μΩ·m) alloys. Such a high electrical resistivity of this alloy explains its low total magnetization losses, including low eddy current losses when used in transformer and choke cores at medium and high frequencies [62].

As the annealing temperature increases (as can be seen in Fig. 7), the electrical resistivity of the ribbon begins to decrease rapidly with increasing annealing temperature above 450°C. At a temperature of 600°C, the electrical resistivity decreases to $1.3 \cdot 10^{-6}$ Ω·m, which is one and a half times less than the initial resistance of the ribbon in the unannealed state, and this is obviously due to the complete nanocrystallization of the ribbon [28, 60].

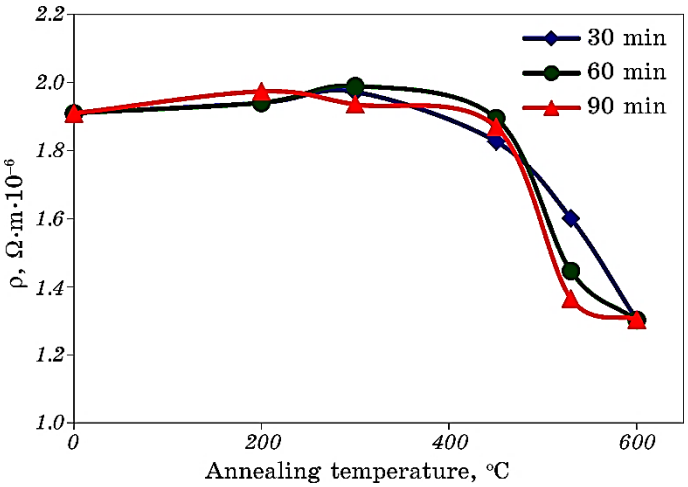

Fig. 7. Dependence of the electrical resistivity of the MM-11H alloy ribbon on the annealing temperature and time.

3.4. Grindability of the Ribbon

For a practical study of the grindability of the ribbon, it was ground in a ball mill for 1 hour in an alcohol medium. For this, the ribbon was first annealed at temperatures of 200, 300, 450, and 530°C, grinded, and then the resulting powder was sieved into fractions with different sets of sieves.

The morphology and shape of the powder particles obtained after grinding the ribbon are shown in Fig. 8.

As can be seen from the photo, all powder particles have a lamellar (flake) shape, which indicates brittle destruction of the alloy.

The results of the sieve analysis are shown in Fig. 9. Analysis of the data shows that with increasing annealing temperature, the grindability of the ribbon increases and the content of fine fractions increases. At an annealing temperature of 200°C, large fractions with a powder particle size of 0.4 to 7 mm predominate, which indicates insufficient

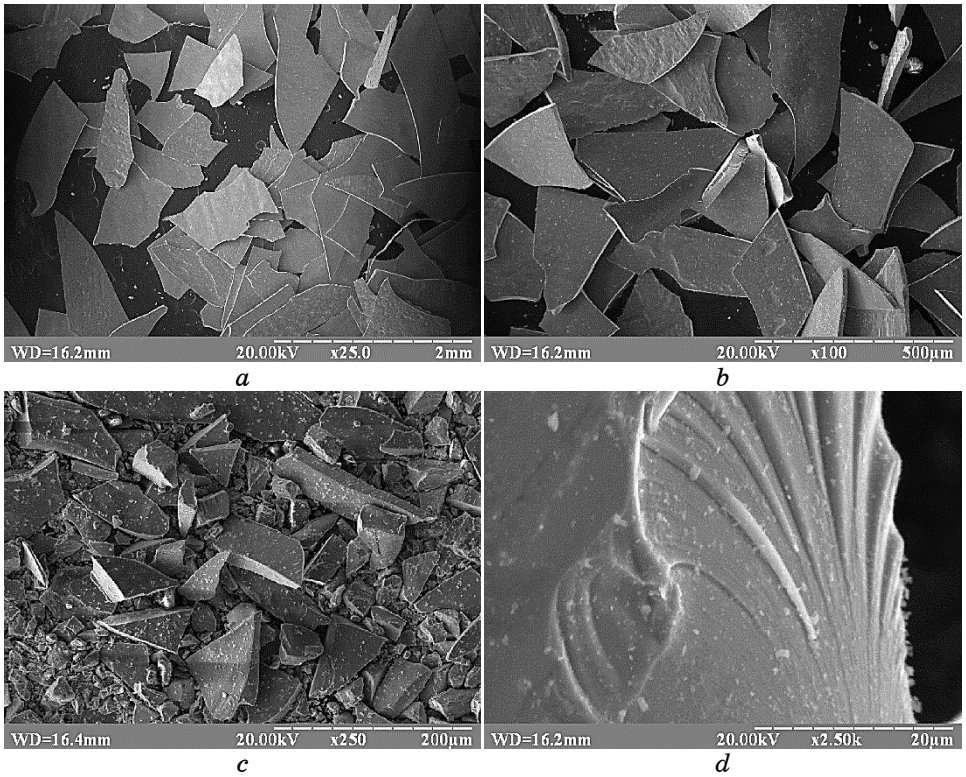

Fig. 8. Shape of MM-11H alloy powder particles from the ribbon annealed at 450°C: fraction 500–2500 µm (*a*), fraction 80–160 µm (*b*), fraction < 50 µm (*c*), fracture surface (*d*).

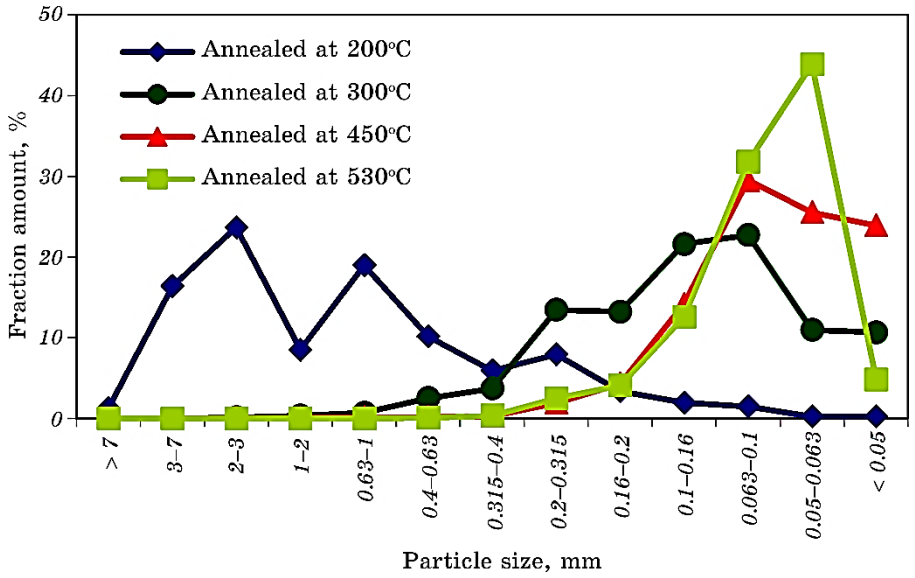

Fig. 9. Fractional composition of the MM-11H nanocrystalline alloy powder after 1 hour of grinding from an amorphous ribbon annealed at temperatures of 200–530°C.

brittleness of the alloy. Such fractions are usually not used for the production of magnetodielectrics, as they are poorly pressed. At an annealing temperature of 300°C, fractions with particles of 0.2–0.063 mm in size predominate, which is already a technologically acceptable size for pressing and manufacturing magnetic conductors. The smallest powder fractions were obtained from the ribbon annealed at 450°C (with the main content of the fraction less than 0.1 mm).

However, at 530°C, a decrease in the amount of the smallest fractions (less than 50 μm) is observed, which may be associated with the deformation hardening of the ribbon when it contains 75–80% of the volume of nanocrystals [60], which negatively affects its grindability.

The practical significance of the results obtained, presented in Figs. 5, 6, and 8, lies in establishing the optimal regimes of pre-annealing and grinding of the amorphous ribbon to obtain an amorphous-nanocrystalline powder of the required (adjustable) fractional composition with minimal microhardness (lower microhardness—better pressing ability of the powder) and the highest electrical resistance (which reduces eddy current losses).

4. CONCLUSIONS

It is shown that the annealing temperature is a key factor that affects

the physical and mechanical properties of the amorphous ribbon of the $Fe_{73}Si_{16}B_7Cu_1Nb_3$ (MM-11H) alloy.

It is established that with increasing pre-annealing temperature above 200°C, the amorphous ribbon almost completely loses its plasticity and turns into a brittle state. In this case, as well as in the annealing temperature range up to 450°C, the microhardness of the ribbon remains practically unchanged (800 kg/mm^2), while an increase in temperature to 600°C leads to an increase in it by almost 2 times.

At the same time, with increasing annealing temperature above 450°C, there is a decrease in the electrical resistivity from $1.9 \cdot 10^{-6}$ μΩ·m to $1.3 \cdot 10^{-6}$ μΩ·m after heat treatment at 600°C, which is caused by the development of nanocrystallization processes in the amorphous ribbon. This value of the electrical resistivity of the nanocrystalline ribbon of the MM-11H alloy is significantly higher than that of industrial crystalline soft magnetic alloys, which are used as a material for the manufacture of magnetic conductors. Such a high specific electrical resistance of this alloy leads to a low level of watt losses for eddy currents when used in transformers and chokes at medium and high frequencies.

It is established that the highest grindability of the amorphous ribbon is achieved after its heat treatment in air at 450°C for 30 minutes. As a result of such treatment, a powder fraction of the smallest size was obtained 100 ± 50 μm.

The results of this study are already being used by the authors to optimize the processes of manufacturing metal-polymer magnetodielectrics based on the nanocrystalline powder of the $Fe_{73}Si_{16}B_7Cu_1Nb_3$ (MM-11H) alloy, as well as in the development of new soft magnetic nanostructured alloys with improved magnetic properties.

REFERENCES

1. O. Gutfleisch, M. Willard, E. Brück, C. Chen, S. Sankar, and J. P. Liu, *Adv. Mater.*, **23**, Iss. 7: 821 (2011).
2. A. M. Leary, P. R. Ohodnicki, and M. E. McHenry, *JOM*, **64**: 772 (2012).
3. S. Wu, W. Hu, Q. Ze, M. Sitti, and R. Zhao, *Multifunctional Mater.*, **3**, No. 4: 042003 (2020).
4. A. Talaat, M. V. Suraj, K. Byerly, A. Wang, Y. Wang, J. K. Lee, and P. R. Ohodnicki, *J. Alloys Compd.*, **870**: 159500 (2021).
5. T. N. Lamichhane, L. Sethuraman, A. Dalagan, H. Wang, J. Keller, and M. P. Paranthaman, *Mater. Today Phys.*, **15**: 100255 (2020).
6. Q. Lu, K. Choi, J.-D. Nam, and H. J. Choi, *Polymers*, **13**, Iss. 4: 512 (2021).
7. J. M. Silveyra, E. Ferrara, D. L. Huber, and T. C. Monson, *Science*, **362**: eaao0195 (2018).
8. *Interdisciplinary Engineering Sciences Concepts, Researches and Applications* (Ed. S. Islak) (Lyon: 2022).
9. B. S. Baitalyuk, V. A. Maslyuk, S. B. Kotlyar, and Ya. A. Sytnyk, *Powder Metall. Met. Ceram.*, **55**: 496 (2016).

10. J. L. Ni, F. Duan, S. J. Feng, F. Hu, X. C. Kan, and X. S. Liu, *J. Alloys Compd.*, **897**: 163191 (2022).
11. G. E. Fish, *Proc. IEEE*, **78**, No. 6: 947 (1990).
12. W. Li, Y. Zheng, Y. Kang, A. Masood, Y. Ying, J. Yu, J. Zheng, L. Qiao, J. Li, and S. Che, *J. Alloys Compd.*, **819**: 153028 (2020).
13. G. Ouyang, X. Chen, Y. Liang, C. Macziewski, and J. Cui, *J. Magn. Magn. Mater.*, **481**: 234 (2019).
14. B. D. Cullity and C. D. Graham, *Introduction to Magnetic Materials* (John Wiley and Sons: 2011).
15. F. Fiorillo, *Characterization and Measurement of Magnetic Materials* (Academic Press: 2004).
16. Z. Y. Wu, Z. Jiang, X. A. Fan, L. J. Zhou, W. L. Wang, and K. Xu, *J. Alloys Compd.*, **742**: 90 (2018).
17. Z. Zheng, S. Li, and K. Peng, *J. Magn. Magn. Mater.*, **568**: 170423 (2023).
18. D. Azuma, N. Ito, and M. Ohta, *J. Magn. Magn. Mater.*, **501**: 166373 (2019).
19. R. Hasegawa, *J. Magn. Magn. Mater.*, **324**: 3555 (2012).
20. S. Lu, M. Wang, and Z. Zhao, *J. Non-Cryst. Solids*, **616**: 122440 (2023).
21. X. Wang, Z. Lu, C. Lu, G. Li, and D. Li, *J. Iron Steel Res. Int.*, **21**: 1055 (2014).
22. C. Chang, J. Guo, Q. Li, S. Zhou, M. Liu, and Y. Dong, *J. Alloys Compd.*, **788**: 1177 (2019).
23. R. Ma and P. Yu, *Mater. Res. Bull.*, **139**: 111256 (2021).
24. H. Shokrollahi and K. Janghorban, *J. Mater. Process. Technol.*, **189**, Iss. 1–3: 1 (2007).
25. A. Krings, A. Boglietti, A. Cavagnino, and S. Sprague, *IEEE Trans. Ind. Electron.*, **64**, Iss. 3: 2405 (2017).
26. K. L. Alvarez, H. A. Baghbaderani, J. M. Martín, N. Burgos, M. Ipatov, Z. Pavlovic, and J. Gonzalez, *J. Magn. Magn. Mater.*, **501**: 166457 (2020).
27. Y. Yoshizawa, S. Fujii, D. H. Ping, M. Ohnuma, and K. Hono, *Scr. Mater.*, **48**, Iss. 7: 863 (2003).
28. *Handbook of Magnetic Materials. Vol. **10*** (Ed. K. H. J. Buschow) (Elsevier: 1997).
29. Y. Yoshizawa, S. Oguma, and K. Yamauchi, *J. Appl. Phys.*, **64**: 6044 (1988).
30. M. Manivel Raja, N. Ponpandian, B. Majumdar, A. Narayanasamy, and K. Chattopadhyay, *Mater. Sci. Eng. A*, **304–306**: 1062 (2001).
31. G. Herzer, *Acta Mater.*, **61**, Iss. 3: 718 (2013).
32. H. Sun, C. Wang, J. Wang, M. Yu, and Z. Guo, *J. Magn. Magn. Mater.*, **502**: 166548 (2020).
33. Z. Guo, J. Wang, W. Chen, D. Chen, H. Sun, Z. Xue, and C. Wang, *Mater. Des.*, **192**: 108769 (2020).
34. T. Zhou, Y. Liu, R. Wang, J. Ye, J. Li, W. Zhao, and V. G. Harris, *J. Alloys Compd.*, **791**: 1138 (2019).
35. C. Wu, H. Chen, H. Lv, and M. Yan, *J. Alloys Compd.*, **673**: 278 (2016).
36. H. Chen, J. Xu, C. Wang, R. Fu, Z. Fu, Q. Chen, and X. Liu, *Ceram. Int.*, **50**, Iss. 19, Pt. A: 35746 (2024).
37. H. Wei, H. Yu, Y. Feng, Y. Wang, J. He, and Z. Liu, *Mater. Chem. Phys.*, **263**: 124427 (2021).
38. X. Li, Y. Dong, X. Liu, S. Wu, R. Zhao, H. Wu, W. Gao, A. He, J. Li, and X. Wang, *Mater. Sci. Eng. B*, **285**: 115965 (2022).
39. B. Wang, Z. Zhang, J. Shen, Y. Tian, B. Wang, L. Cai, L. Liu, Y. Yu, and

G. Wang, *J. Alloys Compd.*, **972**: 172812 (2024).
40. K. J. Sunday and M. L. Taheri, *Metal Powder Rep.*, **72**, Iss. 6: 425 (2017).
41. H. G. Rutz, F. G. Hanejko, and G. W. Ellis, *PM2TEC '97: Powder Metallurgy and Particulate Materials (June 29–July 2, 1997)* (Chicago: 1997).
42. W. Lu, B. Yan, and R. Tang, *J. Alloys Compd.*, **425**: 406 (2006).
43. P. Wang, Z. Zhu, J. Liu, H. Wang, J. Pang, and J. Zhang, *J. Magn. Magn. Mater.*, **596**: 171985 (2024).
44. E. Périgo, B. Weidenfeller, P. Kollár, and J. Füzer, *Appl. Phys. Rev.*, **5**: 031301 (2018).
45. M. Liu, K. Huang, L. Liu, T. Li, P. Cai, Y. Dong, and X.-M. Wang, *J. Mater. Sci. Mater. Electron.*, **29**: 6092 (2018).
46. I. Otsuka, K. Wada, Y. Maeta, T. Kadomura, and M. Yagi, *IEEE Trans. Magn.*, **44**, Iss. 11: 3891 (2008).
47. L. Zhang, Y. Wu, Y. Dong, X. Jia, A. He, J. Li, W. Wang, and B. Shen, *J. Mater. Sci.*, **59**: 8784 (2024).
48. V. A. Maslyuk, B. S. Baitalyuk, and V. K. Nosenko, *Naukovi Notatky. Inzhenerna Mekhanika*, **25**, No. 2: 150 (2009) (in Ukrainian).
49. P. Gramatyka, R. Nowosielski, P. Sakiewicz, and T. Raszka, *J. Achiev. Mater. Manuf. Eng.*, **150**, Nos. 1–2: 27 (2006).
50. P. Gramatyka and R. Nowosielski, *Advances in Nanostructured Materials, Processing–Microstructure–Properties NANOVED 2006–NENAMAT (May 14–17, 2006)* (Bratislava: Slovak Academy of Sciences: 2006), p. 81.
51. F. Mazaleyrat and L. Varga, *J. Magn. Magn. Mater.*, **215–216**: 253 (2000).
52. B. Zhou, M. Lv, J. Wu, B. Ya, L. Meng, L. Jianglin, and X. Zhang, *Mater.*, **15**: 2558 (2022).
53. R. M. Aranda, R. Astacio, P. Urban, B. Aranda, and F. G. Cuevas, *Powder Technol.*, **441**: 119816 (2024).
54. *Melta* www.melta.com.ua.
55. H. Watanabe, *Powder Technol.*, **104**, Iss. 1: 95 (1999).
56. A. M. Glezer and N. A. Shurygina, *Amorfno-Nanokristallicheskie Splavy* [Amorphous-Nanocrystalline Alloys] (Moskva: Fizmatlit: 2013) (in Russian).
57. V. V. Maslov, V. K. Nosenko, L. E. Taranenko, and A. P. Brovko, *Fiz. Met. Metalloved.*, **91**, No. 5: 47 (2001) (in Russian).
58. V. V. Nemoshkalenko, L. E. Vlasenko, A. V. Romanova, V. V. Maslov, V. K. Nosenko, and A. P. Brovko, *Metallofiz. Noveishie Tekhnol.*, **20**, No. 6: 22 (1998).
59. S. P. Hozhii, *Osnovy Fizyko-Tekhnichnykh ta Khimiko-Termychnykh Protsesiv dlya Pidvyshchennya Resursu Vyrobiv Mashynobuduvannya* [Basics of Physico-Technical and Chemical-Thermal Processes for Increasing the Resource of Mechanical Engineering Products] (Kyiv: National Technical University of Ukraine 'Igor Sikorsky Kyiv Polytechnic Institute': 2022) (in Ukrainian)
60. J. Zhou, J. You, and Q. Keqiang, *J. Appl. Phys.*, **132**: 040702 (2022).
61. C. Minnert, M. Kuhnt, S. Bruns, A. Marshal, K. G. Pradeep, M. Marsilius, E. Bruder, and K. Durst, *Mater. Des.*, **156**: 252 (2018).
62. V. K. Nosenko, *Visnyk Natsionalnoi Akademii Nauk Ukrainy*, **4**: 68 (2015) (in Ukrainian).
63. M. P. Semenko, M. I. Zakharenko, Yu. A. Kunytskyi, V. A. Makara, and A. P. Shpak, *Usp. Fiz. Met.*, **10**: 131 (2009) (in Ukrainian).